NUMERICAL MODELLING OF VENTED LEAN HYDROGEN DEFLAGATIONS IN AN ISO CONTAINER

Vendra C. Madhav Rao[1] and Jennifer X. Wen[1]
[1]Warwick FIRE, School of Engineering, University of Warwick, Coventry CV4 7AL, UK
jennifer.wen@warwick.ac.uk

ABSTRACT

Hydrogen process equipment are often housed in 20-foot or 40-foot container either be at refueling stations or at the portable standalone power generation units. Shipping Container provide an easy to install, cost effective, all weather protective containment. Hydrogen has unique physical properties, it can quickly form an ignitable cloud for any accidental release or leakages in air, due to its wide flammability limits. Identifying the hazards associated with these kind of container applications are very crucial for design and safe operation of the container hydrogen installations. Recently both numerical studies and experiment have been performed to ascertain the level of hazards and its possible mitigation methods for hydrogen applications. This paper presents the numerical modelling and the simulations performed using the HyFOAM CFD solver for vented deflagrations processes. HyFOAM solver is developed in-house using the opensource CFD toolkit OpenFOAM libraries. The turbulent flame deflagrations are modelled using the flame wrinkling combustion model. This combustion model is further improved to account for flame instabilities dominant role in vented lean hydrogen-air mixtures deflagrations. The 20-foot ISO containers of dimensions 20’ x 8’ x 8’.6” filled with homogeneous mixture of hydrogen-air at different concentration, with and without model obstacles are considered for numerical simulations. The numerical predictions are first validated against the recent experiments carried out by Gexcon as part of the HySEA project supported by the Fuel Cells and Hydrogen 2 Joint Undertaking (FCH 2 JU) under the Horizon 2020 Framework Programme for Research and Innovation. The effects of congestion within the containers on the generated overpressures are investigated. The preliminary CFD predictions indicated that the container walls deflections are having considerable effect on the trends of generated overpressures, especially the peak negative pressure generated within the container is overestimated. Hence to account for the container wall deflections, the fluid structure interactions (FSI) are also included in the numerical modelling. The final numerical predictions are presented with and without the FSI. The FSI modelling considerably improved the numerical prediction and resulted in better match of overpressure trends with the experimental results.

Keywords: Vented deflagrations, Hydrogen, OpenFOAM, Flame Wrinkling Model, 20-ft ISO container, FSI

1.0 INTRODUCTION

Hydrogen is a clean energy carrier, possible alternative for reduction in the greenhouse gas emissions from the usage of fossil fuels. The use of hydrogen as fuel is steadily on increase in automotive and portable power generation units based on fuel cell technologies. Often 20-foot or 40-foot shipping containers are involved in housing portable hydrogen fuel cell power units and other accessories, even in case of the hydrogen refuelling station, the compressor, pumps and other auxiliary units are housed in these container units. The primary reasons being, shipping containers are durable. Easy to install and provide all weather protection to the process equipment. Hydrogen gas as unique physical properties: low minimum ignition

energy, high diffusivity and wide flammability limits, therefore it can quickly form an ignitable cloud for any accidental release or process leakages in air, subsequent ignition can lead to explosions i.e. rapid combustion of a flammable gas mixture releasing heat, hot combustion products and shock waves. For the process safety, hazards identification and consequence analysis is essential to safeguard these hydrogen installations to mitigate any potential catastrophic accident. The confinement further adds to the generated overpressure magnitudes due to containment of hot combustion products. In case of an accidental gas deflagrations in confinement, venting of these hot gases at a rate greater than the rate of generation of these hot gases will considerably reduce the damage to process equipment and can maintain the structural integrity of the enclosures.

Many experimental studies have been performed in last few decades to understand the process of vented deflagrations [1-5]. Most of the experiments have been done with hydrocarbons as fuel and very few with hydrogen gas. Hydrogen's unique physical properties can influence the vented deflagration processes; hence particular attention is also paid to understand the vented lean hydrogen deflagrations [5-8]. The ratio of thermal diffusivity to mass diffusivity is expressed as Lewis number (Le), it plays an important role in flame propagation in lean hydrogen-air mixtures [9-10]. To account for it, an appropriate 'Le' factor is added to the most of lean hydrogen turbulent flame speed correlations. Flame instabilities also have a dominating effect on vented deflagrations process apart from the flame-turbulence interactions [5-6]. Both thermodynamic and hydrodynamic instabilities influence the process at different stages of the flame evolution. Hydrodynamic Darrieus-Landau and thermo-diffusive instabilities are predominant at the early stages of the flame propagation, leading to cellular and wrinkled flame front. While venting of hot gases occurs through vent opening, Helmholtz oscillations are generated within the enclosure due to inertial effects of the expelled gases and the nozzle effect at vent results in flame and hot combustion product accelerations into relatively cold outside ambient conditions, give rise to Rayleigh-Taylor instabilities at the flame interface. These instabilities coexist in nature, but for the sake in ease of implementation are mostly modelled numerical as mutually exclusive events using either an algebraic expression or solving a transport equation [5-6]. Overall in vented deflagrations process flame propagates in turbulent flows, various flame instability effects combine with the effects due to flow turbulence create the fast deflagrations.

The container applications for hydrogen installations are comparatively new. One of such deflagration experiments in inhomogeneous hydrogen-air clouds in a standard 20′ ISO container are reported by [11]. The effect of nozzle configuration, jet direction, reservoir back pressure, time of ignition after release and degree of obstacles were studied in the experiments. It was found that the overpressures in the experiments without obstacles were in the range of 0.4–7 kPa and with obstacles the gas exploded more violently producing an overpressure in order of 100 kPa. Hence any accidental deflagrations in a container with process equipment inside it will be very catastrophic to workers and public around and necessary mitigating provisions should be incorporated in the design of such container installations.

Recently some experiments have been carried out for homogenous mixtures in full scale 20 foot ISO container configuration by Gexcon [12] as part of the HySEA project supported by the Fuel Cells and Hydrogen 2 Joint Undertaking (FCH 2 JU) under the Horizon 2020 Framework Programme for Research and Innovation. It was observed in the experiments that the container corrugated wall were not rigid and structural deformation/vibrations contributed to the overpressure trends. The preliminary CFD predictions also indicated that the container walls deflections are having considerable effect on the trends of generated overpressures, especially the peak negative pressure generated within the container is overestimated. Hence to account for the container wall deflections, the

fluid structure interactions (FSI) is necessary in the numerical modelling. The CFD and FE coupled solution are more frequent in wind energy technologies development studies Lin [13], but scarce in vented deflagration studies. One of such study was done by [14], wherein the response of an offshore fire partition wall is studied against dynamic deflagration loads. A full spatial mapping of blast overpressure transients obtained with Computational Fluid Dynamics (CFD) FLACS modelling is used in combination with a Non-Linear Finite Element model IMPETUS Afea solver. Mapping in time and space of the overpressure loads helps increasing the accuracy of the mechanical response. A fully coupled CFD and Finite element analysis (FE) will be very compute intensive especially in LES context, may not be worthwhile considering all other uncertainties associated within the vented deflagration process. A more practical approach will be a simple one-way or two-way structural interactions improving the CFD predictions. The study of steel structures in natural fires was attempted by employing the CFD and FE coupled numerical methods by [15]. In their work one-way coupling is done between CFD and FE by dedicated scripts and compute the heat transfer between gas and solid phase. The emphasis is put on the proper calculation of temperature field inside the structural members and, in particular, the non-uniform temperature distribution inside the sections. The need of hour is to develop such simple approach for the vented deflagration applications. In the present study, numerical modelling and simulations are being conducted to further aid our understanding of the vented gas deflagrations in these container units using the opensource Computational Fluid Dynamics (CFD) code OpenFOAM [16] solver HyFOAM. In the following sections, the combustion model and the sub-model for instabilities are described briefly, followed by experimental and numerical setup discursion and finally the numerical predictions are presented with and without the FSI with conclusion remarks.

2.0 NUMERICAL MODELLING

An in-house Computation Fluid Dynamics (CFD) solver is developed using the open source toolkit libraries of OpenFOAM [16] named as HyFOAM. The governing Navier-Stokes equations are solved in explicit Large Eddy Simulation (LES) context with collocated finite volume mesh. A one equation eddy viscosity model is used for evaluating the subgrid scale (SGS) turbulence [17]. LES resolves the large scales of the motion and models the small scales, which is mainly attractive for capturing the unsteadiness in flow. The pressure velocity coupling is solved in Pressure-Implicit Split Operator (PISO) method. The closure for the subgrid viscosity is computed through a transport equation for subgrid kinetic energy. The advective terms are discretized in second-order accurate limited-linear scheme and the temporal term are discretized using a fully implicit, second-order accurate three-time-level method [16]. Hence rendering the developed HyFOAM solver second-order accurate in both time and space coordinates. The complete set of governing equations are solved sequentially with iteration over the explicit coupling terms to obtain convergence. The segregate approach results in a Courant number restriction [18], a Courant number stability criteria of 0.1 was used in the present numerical simulations

2.1 Combustion model

The LES mesh is much larger than the flame thickness, flame front is not resolved and hence is a subgrid entity. A suitable subgrid reaction model is required to taking into account the SGS characteristic turbulence length scales. The Flame Surface Wrinkling Model developed by [18] is used for simulating the turbulent deflagrations. The Flame Surface Wrinkling Model is based on flamelet concept treating the flame as a thin interface between

burnt and unburnt gases. This interface is corrugated and wrinkled due to contributions factor from the flow turbulence. The flamelet concept treats turbulent flame front as an ensemble of laminar flamelet in turbulent flow field, thus simplifies the turbulent combustion treatment by separating the combustion modelling from the analysis of the turbulent flow field. The unburnt zone volume fraction is denoted as a regress variable (b), representative values of b = 1 in fresh gases and b = 0 in fully burnt gas. The transport equation for the resolved part of regress variable (b) is given as [18,19]:

$$\frac{\partial \bar{\rho}\tilde{b}}{\partial t} + \nabla.\left(\bar{\rho}\tilde{U}\tilde{b}\right) - \nabla.\left(\bar{\rho}\mu_{sgs}\nabla\tilde{b}\right) = -\bar{\rho}_u S_L \Xi \left|\nabla\tilde{b}\right| \tag{1}$$

where, Ξ is subgrid flame wrinkling, can be regarded as the turbulent to laminar flame speed ratio and is formally related to the flame surface density by $\sum = \Xi|\nabla\bar{b}|$. Symbols ($\bar{}$) and ($\tilde{}$) represent the filtered and the density weighted filtering operations respectively. ρ is the density, S_L is laminar flame speed and μ_{sgs} is the subgrid turbulent diffusion coefficient. The subscripts u indicates conditioning on the unburned gases region. The resolved filtered unburned gas volume fraction $\bar{b}$ is related to Favre filtered $\tilde{b}$ through $\bar{\rho}_u\bar{b} = \bar{\rho}\tilde{b}$. The closure for the sub-grid wrinkling (Ξ) can be provided either by a balanced transport equation or by an algebraic expression assuming equilibrium between the source terms, whereas the transport model allows for non-equilibrium effects between the source terms. The transport equation model closure for the Ξ is given in equation 2,

$$\frac{\partial \bar{\rho}\Xi}{\partial t} + \tilde{U}_s.\nabla\Xi = \bar{\rho}G\Xi - \bar{\rho}R(\Xi - 1) + \bar{\rho}\max\left[\left(\sigma_s - \sigma_t\right), 0\right]\Xi \tag{2}$$

where, $\tilde{U}_s$ is the surface filtered local instantaneous velocity of the flame, modelled as :

$$\tilde{U}_s = \tilde{U} + \left(\frac{\bar{\rho}_u}{\bar{\rho}} - 1\right) S_L \Xi n_f - \frac{\nabla.(\bar{\rho}\,\mu_{sgs}\nabla\tilde{b})}{\bar{\rho}\,|\nabla\tilde{b}|} n_f \tag{3}$$

The flame normal is $n_f = \nabla\tilde{b}/|\nabla\tilde{b}|$, σ_S and σ_t are the surface filtered resolved strain-rates relating to the surface filtered local instantaneous velocity of the flame ($\tilde{U}_s$) and surface filtered effective flame velocity of the flame surface ($\tilde{U}_t$), modelled as

$$\sigma_t = \nabla.(\tilde{U} + S_L\Xi\, n_f) - n_f.[\nabla(\tilde{U} + S_L\Xi n_f)].n_f$$

$$\sigma_s = \frac{\nabla.\tilde{U} - n_f.(\nabla\tilde{U}).n_f}{\Xi} + \frac{(\Xi+1)[\nabla.(S_L n_f) - n_f.[\nabla(S_L n_f).n_f]}{2\Xi} \tag{4}$$

The terms $G\Xi$ and $R(\Xi - 1)$ in equation 2 represent the sub-grid turbulence generation and removal rates, with G and R as rate coefficients requiring modelling. The modelling of these terms is based on flame-speed correlation of [19] are shown below

$$G = R\frac{\Xi_{eq} - 1}{\Xi_{eq}} \quad \text{and} \quad R = \frac{0.28}{\tau_\eta}\frac{\Xi^*_{eq}}{\Xi^*_{eq} - 1},$$

$$\Xi_{eq} = 1 + 2(1-b)(\Xi^{*}_{eq} - 1) \text{ and } \Xi^{*}_{eq} = 1 + \frac{0.46}{Le}\mathrm{Re}_t^{0.25}\left(\frac{\hat{u}}{Sl_o}\right)^{0.3} \quad (5)$$

where, τ_n is the Kolmogorov time scale, $\hat{u}$ is the sub grid turbulence intensity and Re_t is the turbulent Reynolds number, Ξ_{eq} is equilibrium wrinkling and Ξ^{*}_{eq} is turbulent flame speed correlation. The modelling of the terms Ξ^{*}_{eq} in equation (5) is improved in present work for lean turbulent premixed combustion by including the Lewis number (Le) factor in the turbulent flame speed correlation. The algebraic reaction rate closure, MFSD proposed in [20] is adopted in the present study. This model has been successfully applied to both pure and mixed fuels, under varying Lewis number conditions [10] [21] [22], in both RANS and LES contexts. Figure 1 shows the MFSD model predictions for the turbulent flame speed (S_T) for lean equivalence ratio between 0.4 and 0.8 along with Goulier's expression [23] is compared with the experimental measured values of [24].

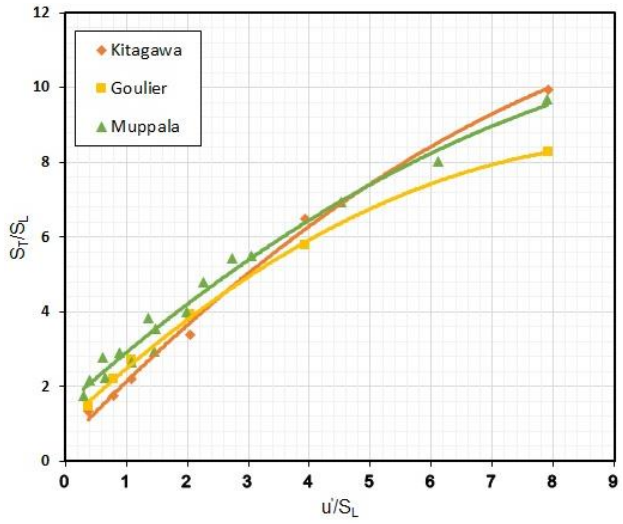

Figure 1. Comparison of turbulent flame speed correlation of [20] [23] with the experimental results of [24].

The Darrieus–Landau and thermodiffusive instabilities affects the flame propagations in lean mixtures leading to formation of cusps and turfs, cellular structures at the flame front. These instabilities are modelled considering the simple analytical expression proposed by [7] as,

$$\Xi_{DL} = \max\left[1, \alpha_1\left(\frac{\Delta}{\lambda_c}\right)^{1/3}\right] \quad (6)$$

where, λ_c is cutoff wavelength of unstable scales and α_1 is a coefficient to account for uncertainty in λ_c, Δ is the LES filter size. The values of λ_c=7mm and α_1=1.3 are used in the current simulations to match the initial flame propagations [7]. The Rayleigh-Taylor instability is modelled as transport equation similar in lines to the equation 2, purposed in [7] is shown below,

$$\frac{\partial \bar{\rho}\Xi_{RT}}{\partial t} + \tilde{U}_s.\nabla\Xi_{RT} = \bar{\rho}G_{RT}(\Xi_{RT}-1) - \bar{\rho}R_{RT}(\Xi_{RT}-1) \quad (7)$$

where, $G_{RT}(\Xi_{RT}-1)$ and $R_{RT}(\Xi_{RT}-1)$ are rate of generation and removal of sub-grid wrinkling due to RT-instability. The coefficients G_{RT} and R_{RT} are modelled as

$$G_{RT} = 2\left(k_{RT}\frac{\sigma-1}{\sigma+1}\mathrm{v}\,\mathrm{v}\,a.n_f\right)^{1/2} \quad \text{and} \quad R_{RT} = \frac{8\sigma S_L k_{RT}}{\pi} \quad (8)$$

where 'a' is flame acceleration evaluated from the flame displacement velocity, σ is flame expansion ratio, k_{RT} is unstable wavenumber associated with the RT-instability assumed to be constant for a given fuel, value of 6 m^{-1} is used in the present study. Another important modelling input is the flame speed. The unstrained laminar flame speed ($S_{L,0}$) function of equivalence ratio ($\phi = 1/\lambda$) for lean hydrogen-air mixture is adopted based on the numerical study carried out by [25], expressed as power law expression for elevated pressure and temperature as ,

$$S_L = S_{L0}(\lambda, P)\left(\frac{T_u}{T_{uo}}\right)^{\alpha(\lambda,P)} \quad (9)$$

$$S_{LO} = 499.63 - 308.60\lambda + 48.887\lambda^2 - 76.238P + 4.825P^2 + 45.813\lambda P - 2.926\lambda P^2 - 7.163\lambda^2 P + 0.436\lambda^2 P^2$$

$$\alpha(\lambda, P) = 1.85175 - 0.70875\lambda + 0.50171\lambda^2 - 0.19366P + 0.0067834P^2 + 0.27495\lambda P - 0.0088924\lambda P^2 - 0.052058\lambda^2 P + 0.00146015\lambda^2 P^2$$

where, S_L in cm/s , P is pressure in bar and T_u unburnt gas temperature in K. The above correlation is valid between the equivalence ratios (ϕ) of 0.33 and 0.47 (very lean mixtures), pressures range of 1bar ≤ P ≤ 8.5 bar and temperature range of 300 K ≤ T ≤ 800 K, with reference temperature state Tu_0 = 300 K. The flame wrinkling factor is equation (1) is updated with sub-models for flame instabilities as,

$$\Xi = \Xi_t * \Xi_{DL} * \Xi_{RT} \quad (10)$$

The equations 1-10 complete the combustion model description for lean hydrogen mixtures in HyFOAM solver.

2.2 Fluid structure interactions

A fully coupled fluid structure interactions (FSI) in CFD, will have two-way interaction i.e. the influence of the fluid forces on the solid structures and the displacements of the solid boundary on the fluid flows, computed during each numerical timestep iterations, with a suitable interface program to exchange the required parameter values between the fluid and solid regions. In the present study, a pseudo two-way interactions approach is being used to improve the CFD predictions, wherein the structural displacements against the overpressures from the experiments are approximated to a spring-mass-damper motion system, assuming container deflections will be within its elastic limits. The structural displacements are applied

to the container walls through a moving wall boundary condition according to the solution of the spring-mass-damper motion system equation during the deflagration process. The overpressures and wall deflections are computed dynamically during the runtime of the CFD simulations, thus making a fully coupled interaction between the CFD and the enclosing structure. In absence of experimental structural displacements, such information can be generated using CFD overpressure as inputs in any dedicated non-linear FEA software's. Similar to the FLAC-IMPETUS one-way coupled results presented in [26].

The experiments conducted in HySEA Phase-1 homogenous mixtures at Gexcon are 12 in number with containers doors open, back wall ignition, involving change in hydrogen concentration and model obstacles. The concise details about the experiments are presented in the following section 3 and the complete details about the HySEA Phase-1 experimental campaign can be found in the [12]. The Tests 1 & 2, which are repeat experiments at 15% H_2 concentration and Empty container; Test 3 & 4, which are repeat experiments at 15% H_2 concentration with cylinder basket as obstacle, are considered to infer the structural response of the container. Figure 2–5, are plots for the experimental observed overpressure and container side wall deflections for without and with obstacles tests respectively.

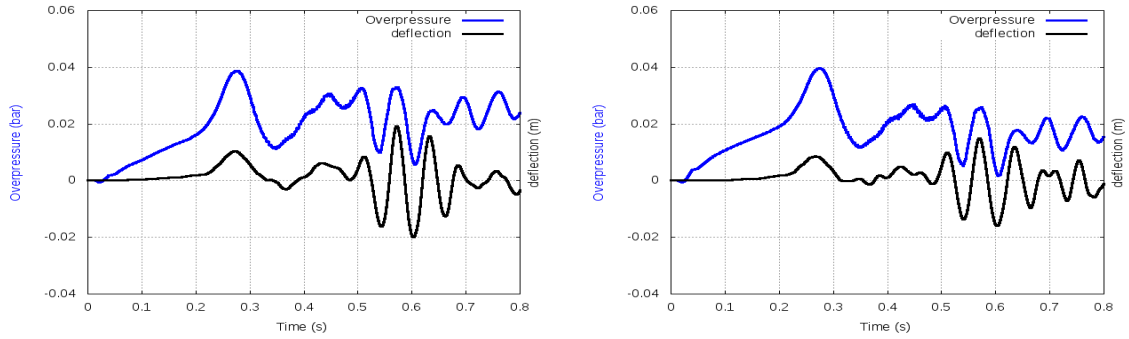

(a) P1 & D1 (b) P2 & D2

Figure 2. For Test -1: 15% H_2, Empty, overpressure and deflection trace curves

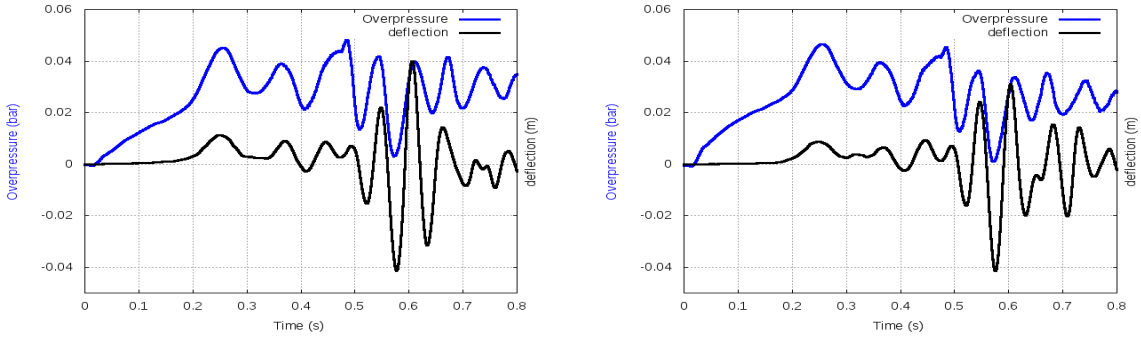

(a) P1 & D1 (b) P2 & D2

Figure 3. For Test -2: 15% H_2 , Empty, overpressure and deflection trace curves

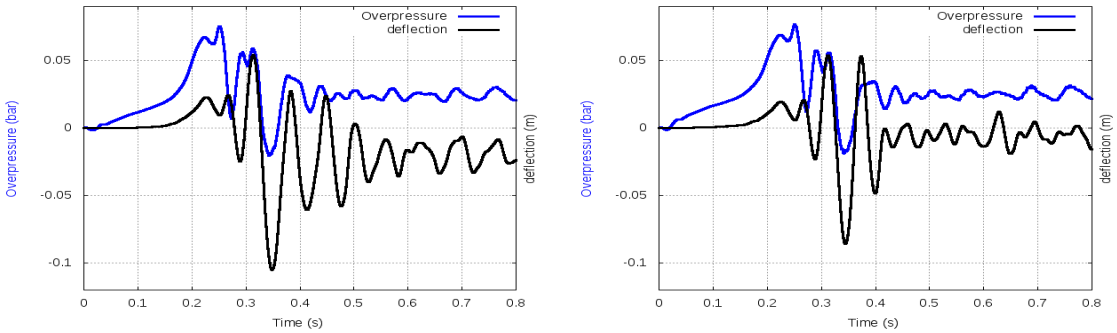

(a) P1 & D1 (b) P2 & D2

Figure 4. For Test - 3: 15% H_2, Cylinder obstacle, overpressure and deflection trace curves

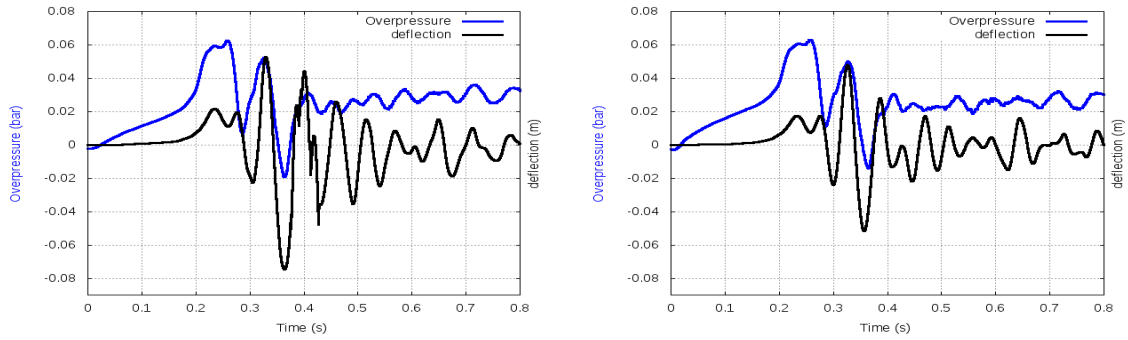

(a) P1 & D1 (b) P2 & D2

Figure 5. For Test - 4: 15% H_2, Cylinder obstacle, overpressure and deflection trace curves

The peak overpressures are recorded at P1 and P2 pressure probe locations for the back wall ignition. The initial rise of the overpressure excites the container wall, which sets the wall into motion, later oscillating in resonance mode. The maximum deflection of container wall is occurring during this resonance phase.

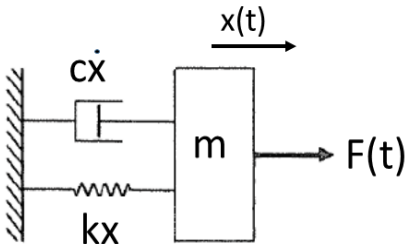

Figure 6. Single degree of freedom motion system

The container wall motion is approximated to a single degree of freedom motion system as shown in Figure 6, this spring-mass-damper system is represented by equation 11.

$$m\frac{d^2x}{dt^2}+c\frac{dx}{dt}+kx=F(t) \tag{11}$$

where, ‘m’ is mass of the system (neglecting the spring mass), ‘c’ is damping coefficient ($Ns.m^{-1}$) and ‘k’ is the spring stiffness factor ($N.m^{-1}$), F(t) is the driving force and x(t) is

response of the system to the driving force (displacements). In the context of the container FSI, F(t) is representative of the mean deflagration overpressure observed at the P1 probe location and x(t) corresponds to the container wall deflections measured by the D1 laser probe. The constants 'm', 'c' and 'k' in equation 11 are estimated to be $6.09x10^{-5}$ kg/m^2, 0.009 N.s/m^3 and 3.84 Pa/m respectively, such that the scaled driving force (i.e. product of F(t) and flexibility factor (1/k)) is in good match with the predicted displacement x(t).

3.0 EXPERIMENTS SETUP

The typical 20-ft ISO container of dimensions 20'x 8'x 8'.6" used in the experiments is shown in Figure 7. The walls of the container are corrugated and 2 mm in thickness. The dimensions of the container inside are 5.867m × 2.385 m × 2.352 m. The container doors are having dimensions of 2.225 m high, 1.114 m wide and 50 mm thick, were kept open in perpendicular position to the container (Figure 9(a)) during the door open venting experiments.

Figure 7. A typical standard 20 ft. ISO container used in the experiments [12].

The open front section of the container is covered with polyethylene sheet to retain the combustible gas mixture, which eventually gets ruptured during the combustion products venting. The homogenous gas mixture inside the container for a given volumetric composition was prepared using recirculation circuit attached to the container. The instrumentation and obstacle are held in a steel frame fixed to the floor of the container. The frame is constructed using U-beams (200 mm x 75 mm) steel sections, shown in Figure 8(b). The two model obstacles, 1) 20 gas bottles held in a basket and 2) pipe rack, first one representative of a dense and later one of a distributive congestion. The individual gas bottles are 50-litre steel cylinders of diameter 0.23 mm and height 1.66 m from the floor to the top of the valve. The cylinders are mounted in a square basket made from 50 mm × 50 mm square steel pipes and the gaps between the bottles spacers fix fixed by spacers to 5 mm. The overall external dimensions of the bottle basket are about 1.27 m × 1.04 m as shown in Figure 8(c).

(a) Wall corrugation

(b) Steel frame (top part)

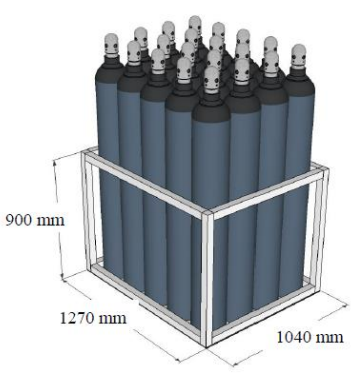

(c) Bottle basket

(d) Pipe rack

Figure 8. Congestion and constrictions with in the containers [12].

The pipe rack obstacle configuration shown in figure 8(b), consists of a frame made using 0.1 m × 0.1 m square steel pipes with dimensions 2.0 m high, 1.3 m long, and 1.1 m wide. This obstacle consists of four layers of pipes laid laterally, the alternative two layers with five 104 mm diameter pipes and other two alternative layers with 2 × 11 pipes with diameter 20 mm each. The pressure sensors are placed symmetrically in the steel frame at distance of 0.86 m for P1&P2, 2.45 m for P3&P4, 4.0 m P5&P6 and 5.56 m for P7&P8 from the backend container wall and 0.2 m elevation from the container floor. The pressure probes placed outside the open doors of the container are at an elevation of 1.65 m and at 5 m (P9), 10 m (P10) and 15 m (P11) distance from the open-end along the centreline, as shown in Figure 9.

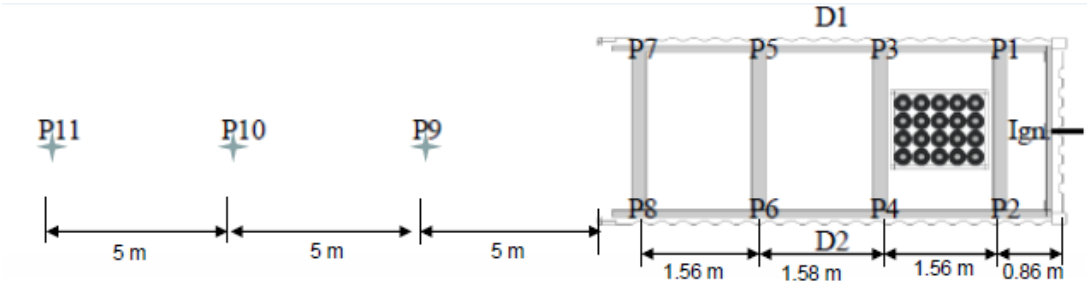

Figure 9. Overpressure monitoring points with respect to the frame and container [12].

The outside container pressure sensors are fitted on to a plate fixed at the top of the vertical tube, about 1.65 m above the ground, measuring the side-on pressure. D1 and D2 are two laser probes pointing the mid-section of either container side wall to measure the container wall deflections with respect to time from start of ignition. An electric inductive spark located at the back wall of the container, along the centreline, and at mid height is used to ignite the homogenous mixtures.

4.0 NUMERICAL SETUP

The standard 20-ft ISO container details considered in the numerical simulation are shown in Figure 10. The series of experiments were conducted by the Gexcon under varying conditions of hydrogen concentration from 15% - 21% by volume, with or without any model obstacles

inside the container. To validate the numerical modelling approach in the present study, three experimental scenarios (case studies) are considered :

1) Case-1: Configuration of no obstacles, steel frame and doors fully open with 15 % hydrogen concentration by volume as shown in Figure 10.

2) Case-2: Configuration with bottle basket close to the back end, steel frame and doors fully open with 15 % hydrogen concentration by volume, shown in Figure 11(a).

3) Case-3: configuration of pipe rack close to the backend, steel frame and doors fully open with 15 % hydrogen concentration by volume, shown in Figure 11(b).

The numerical computational domain with the obstacles inside the container are shown in Figure 11. The ignition of the homogenous hydrogen-air mixture is initiated by a spherical hot patch at the centre of the back end wall at the mid height of the container with products composition and temperature, mimicking the electric spark used in the experiments.

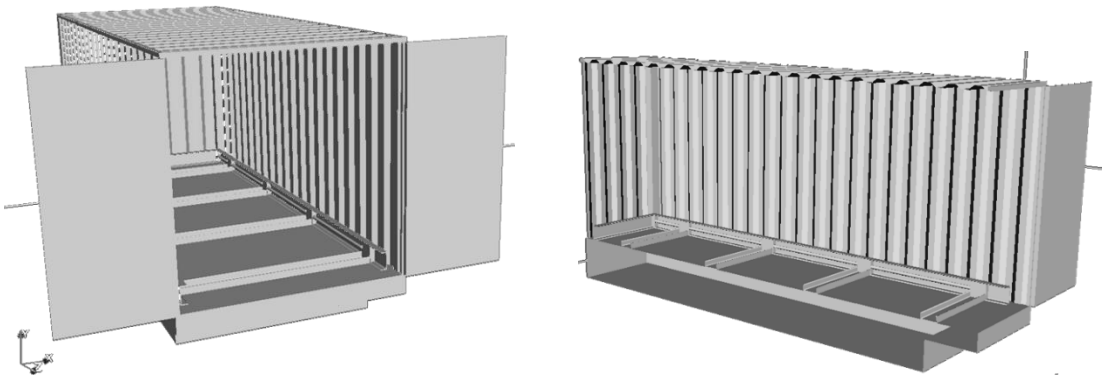

(a) Isometric view (b) Cut section along the centreline

Figure 10. The standard 20-ft ISO container with frame to hold the pressure sensors in the experiments.

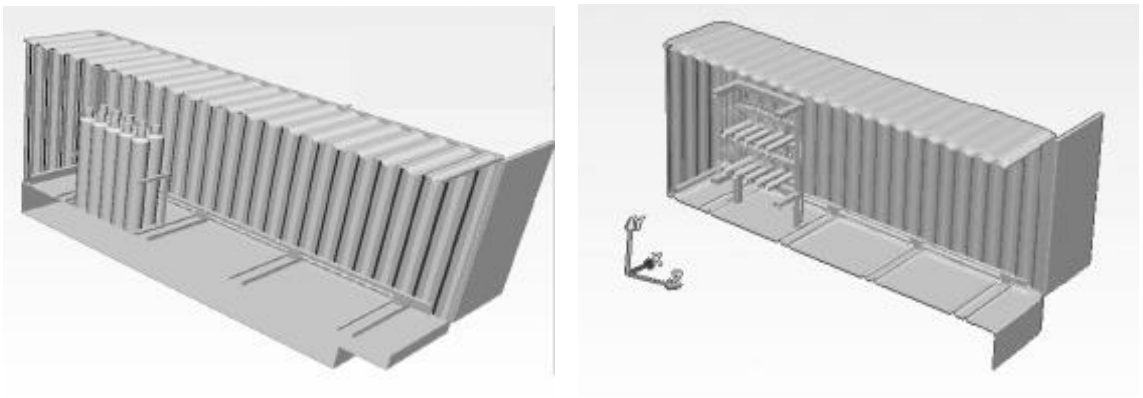

(a) With bottle basket obstacle (b) With pipe rack obstacle

Figure 11. The standard 20-ft ISO container with model obstacles.

The ‘SnappyHexMesh’ utility in OpenFOAM [16] is been used to generate the finite volume, hybrid hexagon/tetrahedral mesh for container geometry. Within the utility a search area is specified along with level of mesh refinement inside it to adequately represent the geometry

features. The non-uniform mesh distribution in the computation domain is shown in Figure 12. The volume enclosing the container, 30.0 m × 15.0 m × 35 m was also meshed to capture the venting of the burnt gas, the external deflagration and to minimise the effect of end boundary conditions on the numerical results. A non-uniform cell size of 5 mm was used in the ignition region, a 5 - 15 mm cell size inside the chamber and in the area immediately outside the chamber to resolve the external deflagration. The total finite volume cells in computational mesh are approximately between 8 ~ 12 million for the three cases considered in the present study.

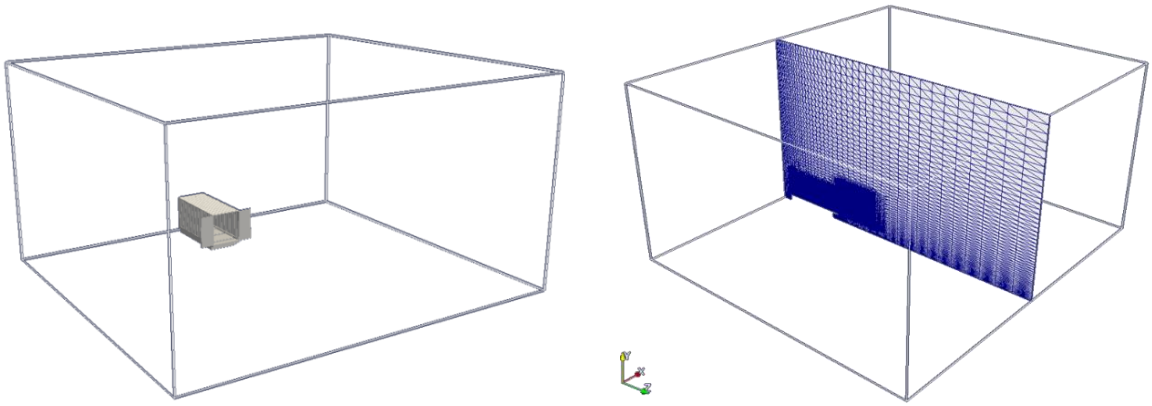

Figure 12. Computational domain and the mesh distribution in vertical cut plane

The container walls are assumed to be rigid initially but later modelled as moving wall to accommodate the Fluid structure interactions (FSI). The boundary conditions applied to the container walls were non-slip, adiabatic walls for the chamber walls and ground. The 'totalPressure' and 'pressureInletOutletVelocity' boundary conditions combination were used for pressure and velocity respectively at the open boundaries. This combination of pressure and velocity boundary condition allows for the flow reversal at the open boundary, i.e. the boundary patch can act as both inlet and outlet based on the fluxes normal to patch-faces, in contrast to outlet boundary which only allow for the domain outward flows. The mixture concentration of 15% volume hydrogen in air is approximately 0.42 equivalence ratio, the unstretched laminar flame speed is around 0.35 m/s, Lewis number is 0.42 and mixture fraction of 0.0122, these values are used in the numerical simulations setup along with an ambient condition of 1 atm pressure and 298 K temperature with no wind conditions. An open vent was used in the simulations with premixed fuel-air mixture initialized in the chamber volume. The random velocity field of the turbulence root mean square velocity u'= 0.1 m/s was initialized in the entire computational domain. Once the wall central deflection is obtained from the overpressure and deflection curves, the displacement contours on each wall surface is applied in the form of an ellipsoidal contours, similar to the results obtained in [26] using the software's FLAC and IMPETUS for CFD and FE calculations respectively, shown in Figure 13. In the Gexcon experiments, it was found that the roof deflection were more than the container side wall deflections due to the difference in the corrugation patterns at roof and side walls. But in the numerical simulations, equal wall deflections are assumed for both container roof and side walls. Figures 14, shows the wall displacement profiles applied in the numerical simulations. The dynamic displacement obtained by solving the equation 11 at the boundary walls based on the overpressure magnitude measured at the probe location P1 & P2 provide the pseudo two way coupling between the CFD and container walls.

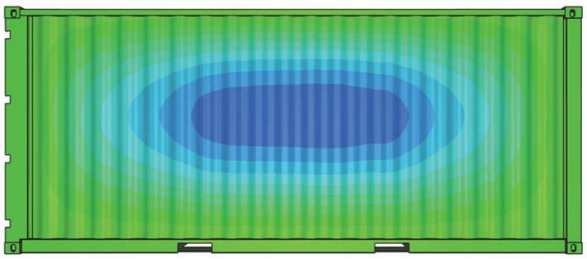

Figure 13. Displacement contours on the side wall of containers [22].

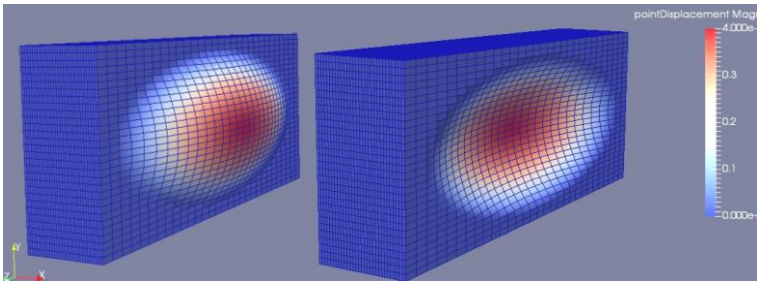

Figure 14. Example for container side wall displacement profiles applied in the numerical simulations for +ve and –ve phase of the overpressure.

5.0 RESULTS AND DISCUSSION

The numerical predictions are plotted along with the experimental measured overpressures in Figure 15, for the case-1 scenario with and without the FSI, i.e., empty container with steel frame at 15 % vol. concentration of hydrogen. The numerical predicted pressure trace curves are low pass filtered at the same frequencies (100 Hz) as applied for the experiment results to smoothen the curve and for getting the mean trends of the overpressure curves. The predicted overpressure trace curves for the pressure probe located within the container for case-1, are shown in Figure 15(a)-(d) and outside in-front of the open container end in Figure 15(e)-(g). The peak pressure is case-1 scenario is obtained at P1 (P2) location. The hot gas continued to expand through the open doors without any flow constriction at the vent section, this leads to decreasing of overpressure trend along the length of the container. The secondary peaks in the pressure trace curves inside the container is much more oscillatory due to the contributions from the Helmholtz oscillation generated by venting of the bulk of the hot gases. The frequency of the oscillations observed in experiments also had the contributions from the structural vibrations of the container walls, which are not present in the without FSI numerical results due to treating the container wall as rigid in the numerical simulations. One more distinct feature present in the numerical prediction is the large magnitude for the first negative pressure, which is almost absent in the experimental results.

Figure 15, numerical predictions for case-1, with the CFD & FSI coupling along with two repeated experimental test results (pressure probes malfunctioned in the experiments are not plotted). The coupling of CFD results with the FE (structural response) has resulted in a significant improvement in the overpressure trends, especially correcting the negative pressures within the container. There is slight reduction in the peak overpressure predictions in without and with the FSI in the numerical simulations. But still the CFD & FSI combination reproduced the overpressures within the range of experimental variabilities.

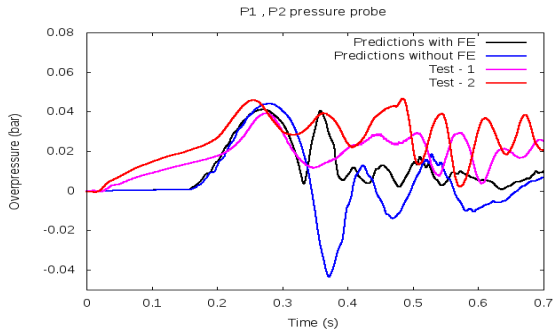
P1 , P2 pressure probe
Predictions with FE
Predictions without FE
Test - 1
Test - 2
Overpressure (bar)
Time (s)

(a)

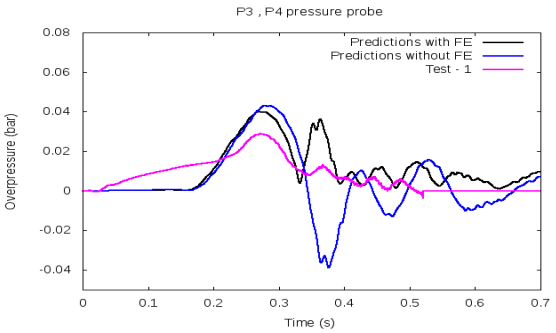
P3 , P4 pressure probe
Predictions with FE
Predictions without FE
Test - 1
Overpressure (bar)
Time (s)

(b)

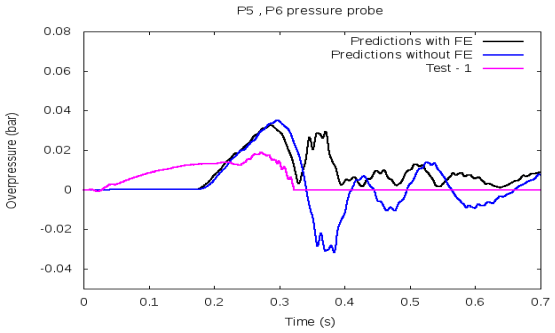
P5 , P6 pressure probe
Predictions with FE
Predictions without FE
Test - 1
Overpressure (bar)
Time (s)

(c)

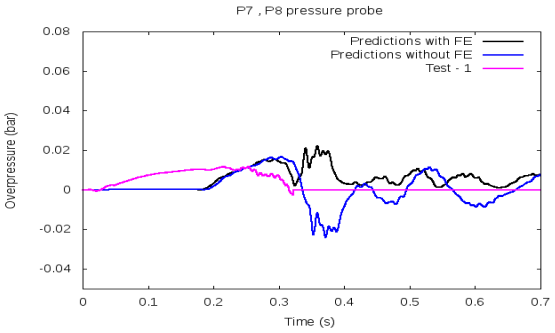
P7 , P8 pressure probe
Predictions with FE
Predictions without FE
Test - 1
Overpressure (bar)
Time (s)

(d)

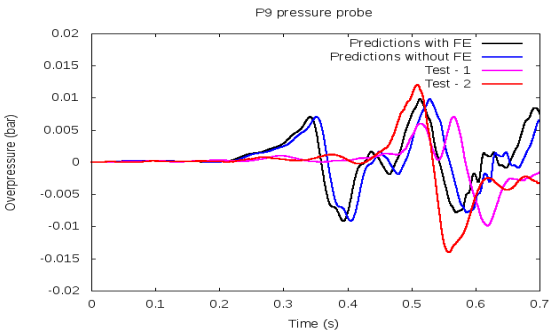
P9 pressure probe
Predictions with FE
Predictions without FE
Test - 1
Test - 2
Overpressure (bar)
Time (s)

(e)

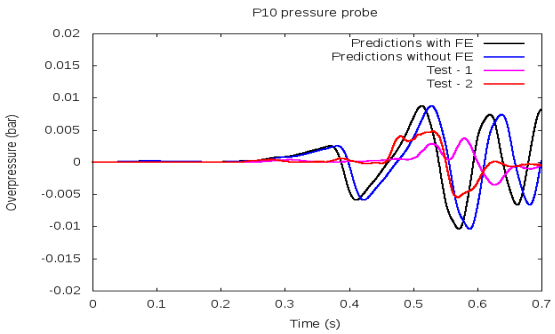
P10 pressure probe
Predictions with FE
Predictions without FE
Test - 1
Test - 2
Overpressure (bar)
Time (s)

(f)

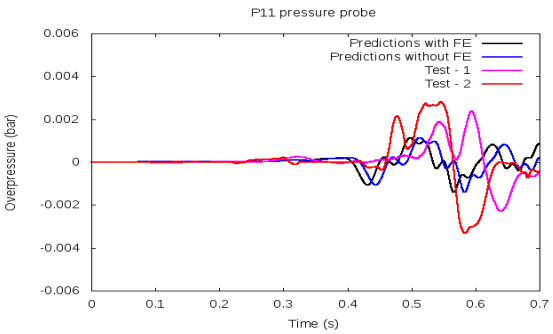
P11 pressure probe
Predictions with FE
Predictions without FE
Test - 1
Test - 2
Overpressure (bar)
Time (s)

(g)

Figure 15. Case-1, pressure trace curves along with Test-1 and Test-2 experimental results, without & with CFD and FSI in pseudo two-way coupling (b, c, d- probes have malfunctioned during the experiments)

The Numerical predictions are presented for the 18% vol concentration hydrogen-air mixture in figure 16. The wall displacements are obtained by solving the equation 11 according to the peak overpressures generated within the container for the 18% vol mixture vented deflagrations.

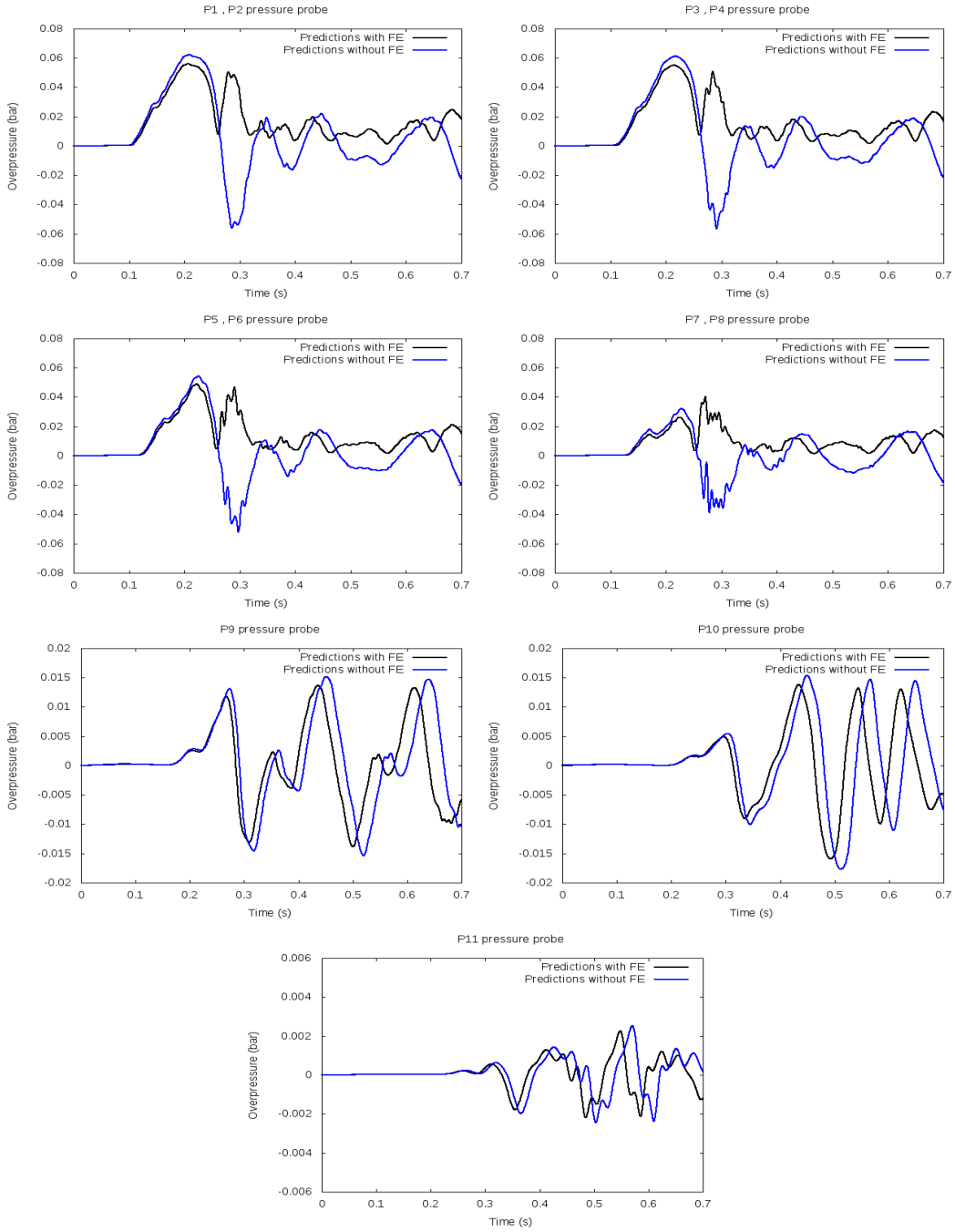

Figure 16. Numerical predictions of overpressures for 18% vol hydrogen mixture, without & with CFD and FSI coupling.

In the Gexcon experimental campaign, the empty container experiments were conducted for 15% hydrogen mixtures concentrations. Hence overpressures trends for other hydrogen concentrations can be generated (like in figure 16: overpressures for the 18% vol hydrogen concentration) using the present coupled CFD and FSI approach.

The Case-2 scenario results are shown in figure 17(a), for the container with steel frame, bottle basket as congestion placed near to the back wall. The overpressures are higher in magnitude than that observed in the base case. The peak pressure is case-2 scenario is also obtained at P1 (P2) location. The hot gas expanded through the open doors, trends in reduced overpressure towards the open-end of the container. The increase in magnitude of the overpressure compared to the empty container results shows the influence of the bottle basket congestion on the flame propagation. The acceleration of the flame around the obstacles leads to generation of higher overpressures. The obstacles contribute in increasing the flame surface area due to flame stretch and straining around them thereby increasing flame consumption rate.

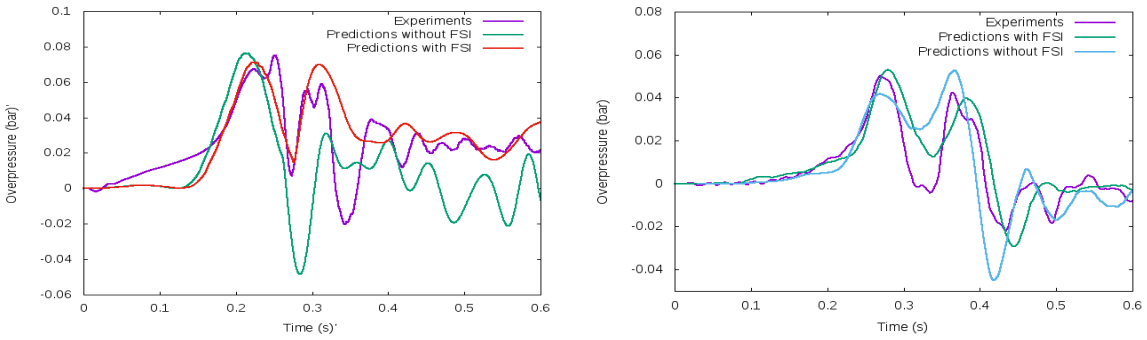

(a) Overpressure trace curve at P1 location (b) Time averaged profile inside the container

Figure 17. Pressure trace curve for P1 pressure probe location along with experiment measurements in case-2 & case3 scenario with bottle basket and pipe rack as obstacles.

Case-3, scenario results are shown in figure 17(b), contains steel rack, pipe rack as obstacles for P1 pressure probe location. The initial pressure rise and the first peak overpressure are captured with in the experimental variabilities in the numerical predictions. The peak overpressure at P1 (P2) only are compared for both the obstacle cases, as the remaining probe located inside the container malfunctioned during the experiments. The bottle basket more over acts like a single large obstacles and the pipe rack acts more like a distributed and porous obstacle, still they both contributed to almost the same rise in overpressure. Although one can argue that the pipe rack should contribute for generation of higher overpressure due to possibility of creating larger flame surface area, the similarity in trends of the overpressures in case-2 and case-3 could be due to the placement of obstacles closer to the ignition location and hence enough flame surface area was not generated before actual interactions of the flame with the obstacles happened. Although the pressure trace curves locally vary in profile to that of the experiments but the overall trends in terms of the overpressure magnitudes are well represented in the numerical predictions. The peak overpressures at P1 location in case-2 and case-3 are close to twice in magnitude to that observed in the base case-1 scenario. Clearly the constriction in the flow path of the flame contributed for flame accelerations leading to higher overpressures. The knowledge of these overpressure magnitudes due to contributions from the different process equipment (obstacles) is very essential in designing the vents, allowable

congestion levels and operation safety at the new hydrogen installations, such as the portable self-contained power generation units.

6.0 CONCLUSION

The 20-ft ISO containers are being considered for hydrogen installations either for developing self-contained portable power generation units using the fuel cell technologies or for housing compressor/pumps at hydrogen refueling stations. The possible scenarios of lean hydrogen-air deflagrations in these containers are being studied numerically in the present study. Experimental data from full scale 20-foot container tests carried out by Gexcon, are used for numerical modelling validations. The modification to flame speed correlation and turbulent flame speed considered in the present study result in reasonable accuracy of numerical predictions to experiments. The mesh refinement at the ignition location and tuning of the ignition parameters such as the ignition patch volume, ignition burnt mass fraction and ignition lag resulted in better prediction of initial pressure rise and first peak overpressure. To further improve the overpressure trends, the CFD simulations are coupled to FSI in a pseudo two-way interactions, where in the experimental structural responses are approximated to a spring-mass-damper motion system and dynamically evaluated at the boundary wall to obtain the displacements in response to the peak overpressure inside the container. The final numerical results of the coupled CFD and FSI are very promising in predicting the experimental trends within the experimental uncertainties. The major improvement is in correction of the peak negative pressures observed after the first peak overpressure in the CFD results without the FSI. Shown in Figure 17, the vented deflagrations of 15% vol. concentration of hydrogen in the container with model obstacles produced nearly twice the overpressures in magnitude to that of in the empty container. Such information is very vital in designing the vents in the process equipment and also defining the safety distances around the hydrogen process installations.

Acknowledgements

The HySEA project (www.hysea.eu) receives funding from the Fuel Cells and Hydrogen Joint Undertaking under grant agreement No 671461. This Joint Undertaking receives support from the European Union's Horizon 2020 research and innovation programme and United Kingdom, Italy, Belgium and Norway.

REFERENCES

1. Mccann, P. J., Thomas, G. O., Edwards, D. H. (1985) Geodynamics of Vented explosions Part I: Experimental studies, Combustion and Flame, 59 : 233-250.
2. Cooper, M. G., Fairweather, M., & Tite, J. P. (1986). On the mechanisms of pressure generation in vented explosions. Combustion and Flame, 65(1), 1-14.
3. Molkov, V.V., Baratov, A.N., and Korolchenko, A.Y., Dynamics of gas explosions in vented vessels: a critical review and progress, Progress in Astronautics and Aeronautics, 154: 117-131 (1993).
4. Bauwens, C. R., Chaffee, J., & Dorofeev, S. (2010). Effect of Ignition Location, Vent Size, and Obstacles on vented Explosion Overpressures in Propane-Air Mixtures. Combustion Science and Technology, 182(11), 1915 – 1932.

5. Bauwens, C.R., Chaffee, J., and Dorofeev, S.B., “Experimental and Numerical Study of Hydrogen-Air Deflagrations in a Vented Enclosure,” in 7th ISHPMIE proceedings Vol. 1, St. Petersburg, Russia, 2008.
6. Molkov,V.V, R. Dobashi, M. Suzuki and T. Hirano, Modelling of Vented Hydrogen-Air Deflagrations and Correlations for Vent Sizing, *J. Loss Prev. Process*, **12**, 1999, pp. 147-156.
7. Bauwens, C.R., Chaffee, J., and Dorofeev, S.B., “Vented Explosion Overpressures from Combustion of Hydrogen and Hydrocarbon Mixtures,” IJHE, vol. 36, no. 3, pp. 2329–2336, Feb. 2011.
8. Bauwens, C. R, Dorofeev, S. B, Effect of initial turbulence on vented explosion overpressures from lean hydrogen air deflagrations, Int. Journal of Hyd. Energy, 39, 2014.
9. Abdel-Gayed R. G., Bradley, D, Hamid M., N. Lawes, M., Lewis number effects on turbulent burning velocity (1985), Twentieth Sym. on Combust.
10. Chakarborty, N., Cant, R.S, Effects of Lewis number on flame surface density transport in turbulent premixed combustion (2011). Comb. and Flame. 9:158.
11. Sommersel, O.K., Vaagsaether, K. & Bjerketvedt, D., (2017) Hydrogen explosions in 20 ft ISO container. International Journal of Hydrogen Energy, **42**, pp. 7740-7748.
12. Skjold, Trygve, Hisken, Helene, Lakshmipathy, Sunil, Atanga, Gordon, van Wingerden, Matthijs, Olsen, Kjetil Lien, Holme Morten Norlemann, Turoy, Nils Martin, Mykleby, Martin, Kess,(2017) “Vented hydrogen deflagrations in containers : Effect of congestion for homogenous mixtures”. Zenodo. http://doi.org/10.5281/zenodo.998039.
13. Lin Wang, Robin Quant, Athanasios Kolios, (2016) Fluid structure interaction modelling of horizontal-axis wind turbine blades based on CFD and FEA, Journal of Wind Engineering and Industrial Aerodynamics,Vol 158, p 11-25.
14. Salaun, N., Gronsund A.H. and Nilsen, P.E., (2016) Risk-based Structural Response against Explosion Blast Loads: Systematic One-to-one CFD (FLACS) / NLFEA (IMPETUS Afea Solver) Coupling to Derive Quantified Response Exceedance, Chemical Engineering Transactions, 48, pp. 55-60
15. Michał Malendowski, Adam Glema,(2017) "Development and Implementation of Coupling Method for CFD-FEM Analyses of Steel Structures in Natural Fire", Procedia Engineering,Volume 172, 2017,P 692-700
16. www.openfoam.org.
17. Fureby, C., et al., A comparative study of subgrid scale models in homogeneous isotropic turbulence. Physics of Fluids, 1997. **9**(5): p. 1416-1429.
18. Weller, H. G., Tabor, G., Gosman, A. D., and Fureby, C., Application of a flame wrinkling LES combustion model to a turbulent mixing layer (1998), Proc. of Combust. Inst., 27.
19. Tabor, G. and H.G. Weller, Large Eddy Simulation of Premixed Turbulent Combustion Using Ξ Flame Surface Wrinkling Model. Flow, Turbulence and Combustion, 2004. **72**(1): p. 1-27.

20. Muppala Reddy, S. P., Aluri Naresh K., Dinkelacker, F., Development of an algebraic reaction rate closure for the numerical calculation of turbulent premixed methane, ethylene, and propane/air flames for pressure up to 1.0 MPa (2005), Combust. And Flame, 140.
21. Burke, E., M., Singlitico A., Morones, A., Petersen, E., L., Guthe, F., BiruteBunkute, Speth, R., L., Monaghan, R., F., D., progress towards a validated Cantera-based turbulent flame speed solver (2015), Proc. of the European Combust. Meeting.
22. Muppala, S., P., R., Nakahara, M., Aluri, H., Kido, Wen, J. X, Papalexandris, M. V., Experimental and analytical investigation of the turbulent burning velocity of two-component fuel mixtures of hydrogen methane and propane (2009), Int. Journal of Hyd. Energy, 22:34.
23. Goulier, J. Comandini, A., Halter, F., Chayumeix, N., experimental study on turbulent expanding flames of lean hydrogen/air mixtures (2016), Proc. Combust. Inst.
24. Kitagawa, T., Nakahara, T., Maruyama, K, Kado, K., Hayakawa, A., Kobayashi, S., Turbulent burning velocity of hydrogen-air premixed propagating flames at elevated pressure (2008), Int. Jol. of hyd. Energy, 20:33.
25. Verhelst, S., A laminar velocity correlation for hydrogen/air mixtures at spark ignition engine conditions (2003), Spring Technical Conf. of ASME internal Combust. Engine division, ICE2003.
26. Atanga, Gordon, Lakshmipathy, Sunil, Skjold, Trygve, Hisken, Helene, & Hanssen. (2017), “Structural response for vented hydrogen deflagrations: coupling CFD and FE tools”. Zenodo. http://doi.org/10.5281/zenodo.1165356